

# Investigation of Polybutylene Succinate-co-Adipate (PBSA)/Montmorillonite Layered Silicate (MLS) Melt-Processed Nanocomposites

Diane M. Steeves<sup>1</sup>, Richard Farrell<sup>2</sup>, and Jo Ann Ratto<sup>1,\*</sup>

<sup>1</sup>U.S. Army Natick Soldier Center, Natick, Massachusetts 01760-5020, USA

<sup>2</sup>University of Saskatchewan, Soil Science Department, Saskatoon, S7N 5A8, Canada

Biodegradable nanocomposites were prepared with polybutylene succinate adipate (PBSA) and three organically modified montmorillonite layered silicates (MLSs) by melt-extrusion methods at three screw speeds (20, 40, and 60 rpm) to determine the interaction and properties of the polymer/MLS nanocomposites. The samples were evaluated by X-ray diffraction (XRD) and transmission electron microscopy (TEM) to determine the level of MLS interaction with PBSA. All formulations formed varying degrees of intercalation regardless of the modification of the MLS or the variation of the screw speed upon melt processing. Differential scanning calorimetry (DSC) experiments did not reveal significant differences in melt temperature or glass transition temperature of PBSA. Dynamic mechanical analysis did display improved modulus values as a function of temperature with some of the nanocomposite formulations processed at different screw speeds. Extensive biodegradation tests were performed and determined that the nanoparticles did not hinder biodegradation in soil. Toxicity tests also were performed and all samples proved to be nontoxic.

**Keywords:** Biodegradable Nanocomposites, Extrusion Processing, Environmental Degradability.

## 1. INTRODUCTION

For many years there has been a global effort to develop biodegradable polymers to meet the demand of environmental concerns, legislation, scientific research, and waste management. Currently, both biodegradable and biobased materials have become an area of focus for both industry and government.<sup>1–3</sup> There are many biodegradable and biobased polymers that can be processed into useful packaging items for the military and commercial sectors.<sup>4,5</sup> However, a barrier to the commercialization of biodegradable and/or biobased items is often the combination of price and performance compared to already existing thermoplastic products.

The polymers need to meet performance specifications for particular applications. Many of the existing synthetic biodegradable polymers have low heat deflection temperatures and low end use temperatures.<sup>6</sup> One approach to overcoming these deficiencies is to add montmorillonite layered silicate (MLS) nanoparticles to the biodegradable polymer to produce nanocomposites.

The nanocomposites contain small amounts of MLS (1–5% by weight) and exhibit properties that differ

from those of conventional polymer composites, which contain large amounts of fillers and/or reinforcements. Improvements in the thermal stability, flame resistance, and mechanical and barrier properties of the processed nanocomposites, as well as reduced weight of material required in end-item use, have been reported.<sup>7–9</sup>

Montmorillonite, which consists of nanometer-sized platelets, is the most commonly used organically modified layered silicate material. The platelets impart structural orientation in the samples as the polymer molecules become entwined between the individual layers of the MLS. The platelets measure approximately 1 nm in thickness and 100–200 nm in width and thus possess a high aspect ratio, which is important for barrier properties.<sup>7–9</sup> The high aspect ratios may affect biodegradation rates, since biodegradation is dependent on surface area. The benefit of the MLS is that the surface modifier can be tailored with specific groups that may contribute to the biodegradation rate and the mechanism of biodegradation. In particular, for this study we are using montmorillonites organically modified with aminolauric acid or quarternary amine chloride functionality.

Polymer/MLS nanocomposites can be prepared in several ways. One approach, *in-situ* polymerization, involves dispersing the MLS in a monomer and allowing the

\*Author to whom correspondence should be addressed.

monomer molecules to penetrate into the galleries of the MLSs. Polymerization is then initiated and the polymer is formed in-place within the MLS particles.<sup>10,11</sup> A second approach involves direct mixing and melt processing of the polymer and MLS to diffuse the polymer chains into the MLS platelets.<sup>8,12</sup> The present study focuses on the preparation of PBSA/MLS nanocomposites via the melt processing technique and an investigation of the degree of MLS dispersion to determine the influence of the mixing and processing conditions on the thermal, mechanical, and biodegradation properties of the nanocomposites.

PBSA is an aliphatic thermoplastic polyester that has many interesting properties, including biodegradability, melt processability, and thermal and chemical resistance.<sup>13–16</sup> PBSA is synthesized by the reaction of glycols with aliphatic dicarboxylic acids and is available for use in a variety of applications including films, laminations, sheet extrusion, monofilaments, multifilaments, blow-molded containers, injection molded cutlery, and foam cushions.<sup>13</sup> The succinic acid which is used to prepare this polymer is created by fermentation of sugar extracted from sugarcane or corn, therefore classifying it as a biobased material.<sup>17</sup>

Earlier studies have demonstrated that PBSA, in the form of films and molded objects, exhibits significant biodegradation within 4 months of treatment in soil and water with activated sludge.<sup>14,15</sup> A previous study has focused on the addition of corn starch to the PBSA to generate blends with improved cost competitiveness and biodegradation while maintaining good mechanical properties and processability.<sup>13</sup> It was determined that starch increases the rate of biodegradation and a blend containing 15% starch reaches 60% net mineralization after only 1 month.<sup>13</sup>

Although several articles dealing with PBSA and poly(butylene succinate) (PBS) nanocomposites have been published in recent years,<sup>18–34</sup> none of these studies involved melt-processed films produced from a die. Moreover, biodegradation of the resulting nanocomposites was not extensively studied. Chen et al. have conducted studies of PBS and PBSA with twice functionalized MLS consisting of Southern Clay's Cloisite® 25A and treating that with silane compounds, namely, (glycidylxypropyl) trimethoxysilane or (methacryloyloxypropyl) trimethoxysilane.<sup>18–20</sup> These materials were melt-compounded and then hot-pressed into sheets. The studies evaluated the morphology, as well as the improvement of tensile properties, in the twice-functionalized MLS in comparison to the nanocomposite containing the virgin Cloisite® 25A.<sup>19,20</sup> Chen also studied the nonisothermal crystallization kinetics of these nanocomposites with results indicating that the twice-functionalized MLS had higher nucleation than the Cloisite® 25A nanocomposite for the crystallization of PBS. Another twice-functionalized nanocomposite consisting of poly(L-lactide)/PBS (75/25 w/w) were produced using a similar method. Exfoliated nanocomposites were

achieved containing the twice-functionalized MLS produced sheets with the highest thermal stability.<sup>20</sup>

Ray et al. have published several studies examining structure–property relationships in poly(butylene succinate) (PBS)/MLS systems.<sup>23–25</sup> Several organically modified nanoparticles, including montmorillonite modified with octadecylammonium chloride or octadecyltrimethylammonium chloride and saponite modified with quaternary hexadecyl tri-*n*-butylphosphonium bromide, were investigated. The nanocomposites were prepared by melt extrusion into strands which were then pelletized and pressed into sheets. The mechanical, rheological, and biodegradation properties of the resulting nanocomposites were examined. All the nanocomposites exhibited improvements of mechanical properties in both the solid and melt when compared to pure PBS. The authors attributed these improvements to flocculated intercalates in the nanocomposites. No significant changes in biodegradation were noted for the nanocomposite systems, with the exception of the greater occurrence of cracking in the samples. Ray et al. also investigated several poly(butylene succinate-*co*-adipate) (PBSA)/MLS systems.<sup>23,24</sup> These nanocomposites were prepared as described above, using the commercial montmorillonite clays Cloisite® 30B, 15A, and 93A (Southern Clay Products). Again, improvements in mechanical and rheological properties were seen, and a dependence of the crystallinity on the degree of intercalation was noted. No biodegradation studies were carried out on the PBSA systems.

Someya et al. also studied PBS with a series of non-modified and organically modified amine nanoparticles to study the influence on morphology and dispersion.<sup>26</sup> The samples were injection-molded and then characterized for thermal and mechanical properties. The glass transition temperature and the storage modulus varied depending on the nanoparticle concentration (3–10%). The organically modified nanoparticles incorporated into PBSA showed better tensile properties than the nonmodified nanoparticle nanocomposites.

Lee et al. studied the melt intercalation of PBSA using two Southern Clay Cloisite® nanoparticles: MLS 30B and MLS 10A.<sup>28–30</sup> The PBSA/MLS 30B had better intercalation and mechanical properties than the PBSA/MLS 10A due to strong hydrogen bonds.

Lim et al. published several studies preparing solvent-cast nanocomposites using an aliphatic polyester (Skygreen 2109) with different organically modified MLS.<sup>31–35</sup> In one study, the PBSA was blended with polyepichlorohydrin. These studies focused on the morphology, rheology, and storage and loss moduli of these materials.

The goal of this study was to incorporate nanoparticles to improve thermal and/or mechanical properties as well as to investigate the influence of nanoparticles on polymer biodegradability. The rate and extent of biodegradation depends on polymer structure as well as on conditions in

the disposal environment. Most environmentally degradable polymers biodegrade readily in compost and soil when environmental conditions (i.e., temperature, pH, and moisture) are optimized. A challenge for both the military and commercial sectors is the development of polymers that exhibit appropriate performance properties and that biodegrade readily without releasing toxic products into the environment. In the study presented here, nanocomposites of PBSA with organically modified MLSs were prepared by extrusion methods. The effects of processing conditions and the additions of MLS and/or starch on the improvement of the mechanical properties and dispersion were investigated. The results are instructive on the behavior of these systems and provide guidance for future improvements for processing and characterization of MLS nanocomposites.

## 2. EXPERIMENTAL DETAILS

### 2.1. Materials

The PBSA utilized in these studies was supplied by Showa Denko High Polymer with the trade name Bionolle™ 3001. The structure of this material is shown in Figure 1. The polymer is a film grade with a melt temperature of 100 °C, a glass transition temperature of -45 °C, and a density of 1.2 g/cm<sup>3</sup>. The melt flow index at 190 °C is 1.11, the  $M_n$  is 62 000 g/mol and  $M_w$  is 165 000 g/mol.

A PBSA master batch containing 50% starch was also used to prepare a nanocomposite. The modified MLSs were supplied by Southern Clay Products. The structures are shown in Figure 2 and identified as MLS 1330, MLS 1855, and MLS 1856. MLS 1330 is a modified nanoparticle consisting of a 12-aminolauric ion-exchanged MLS. MLS 1855 is a quarternary amine chloride-exchanged MLS and 1856 is an amino hydrochloride-exchanged MLS. These particular MLSs were chosen due to the differences in functional groups available to react with the polymer and to allow for a structure/function analysis of effect of organic modifier on intercalation and other physical properties. MLS 1330 contains a single reactive group, while MLS 1855 and MLS 1856 each contain two functional groups, as well as a long carbon chain absent in MLS 1330. Additionally, MLS 1855 contains a NH functionality versus MLS1856 with a N-CH<sub>3</sub> functionality.

### 2.2. Extrusion Processing

A series of PBSA/MLS nanocomposites were prepared using twin screw extrusion. For several formulations,

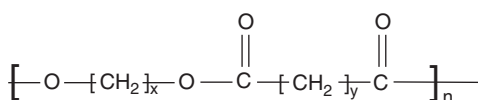


Fig. 1. Structure of PBSA, where  $x = 4$ ,  $y = 2$ , 4.

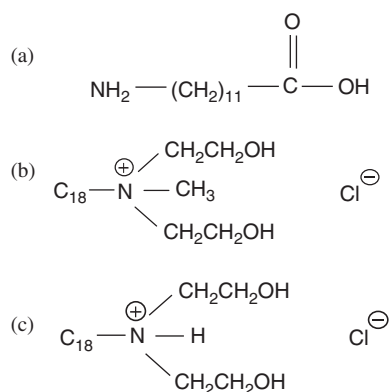


Fig. 2. Structures of the modified MLS: (a) MLS-1330 12-aminolauric acid; (b) MLS-1855 stearyl bis(2-hydroxyethyl)methyl quaternary amine chloride; (c) MLS-1856: stearyl bis(2-hydroxyethyl)amino hydrochloride.

PBSA pellets were cryogenically milled into powders and combined with the MLS powders. Otherwise, the PBSA pellets were combined with the MLS powders. The pure PBSA, processed at 20 rpm, was used as a control throughout this study. The PBSA was processed in both pellet and powder form; however, this had no significant effect on processing or characterization of the resulting samples.

Extruded samples, all containing 5% MLS, were processed with a Haake Rheochord System 40 with a conical twin screw extruder at 20, 40, and 60 rpm using a ribbon die with the following temperatures in zones 1–4, respectively: 150, 160, 175, and 185 °C. The screw diameter was 22 mm. No variations in processing parameters were needed for the different MLS chemistry modifications and

Table I. Materials evaluated in PBSA/MLS nanocomposite study.

ID	Description	% Residue from TGA
1A*	Pure PBSA 3001: 10 rpm	
1D*	Pure PBSA 3001: 20 rpm	
2A*	PBSA (pellet)/MLS 1330: 20 rpm	2.7
2C*	PBSA (pellet)/MLS 1330: 40 rpm	2.5
3A*	PBSA (powder)/MLS 1330: 20 rpm	2.2
3B*	PBSA (powder)/MLS 1330: 40 rpm	3.9
3C*	PBSA (powder)/MLS 1330: 60 rpm	4.5
4B*	PBSA (pellet)/MLS 1855: 20 rpm	3.2
4C*	PBSA (pellet)/MLS 1855: 40 rpm	4.1
4D <sup>†</sup>	PBSA (pellet)/MLS 1855: 60 rpm	4.0
5A*	PBSA (powder)/MLS 1855: 20 rpm	1.5
5B <sup>†</sup>	PBSA (powder)/MLS 1855: 40 rpm	2.1
5D*	PBSA (powder)/MLS 1855: 60 rpm	3.9
6A*	PBSA (powder)/starch/MLS 1855: 20 rpm (50:50 starch:MLS)	4.4%
6C*	PBSA (powder)/starch/MLS 1855: 60 rpm (50:50 starch:MLS)	6.9
7A*	PBSA (pellet)/MLS 1856: 20 rpm	3.6
7C*	PBSA (pellet)/MLS 1856: 40 rpm	3.4
Cell	Microcrystalline cellulose (TLC grade) <sup>†</sup>	

\*Sigma Chemical Corp., St. Louis, MO.

<sup>†</sup>Fully characterized and performed biodegradation and toxicity tests on these samples.

<sup>‡</sup>Fully characterized but did not do biodegradation or toxicity test.

PBSA samples. The formulations processed and analyzed are described in Table I.

### 3. METHODS

#### 3.1. X-Ray Diffraction

X-ray analysis was performed on each PBSA/MLS system processed at the different screw speeds to determine the degree of intercalation and/or exfoliation. The  $d$ -spacings were compared to pure MLS. A Scintag XDS 2000 diffractometer was used at 45 kV and 40 mA power. The slits were tube side with scatter at 4 mm and divergence at 2 mm. The detector side has scatter of 0.5 mm and receiving of 0.2 mm. The analysis was done under normal scan with a start angle of  $1.0^\circ 2\theta$ , stop angle of  $11.98^\circ 2\theta$ , rate of 1 deg/min, and step size of  $0.030^\circ$ .

#### 3.2. Transmission Electron Microscopy

Transmission electron microscopy (TEM) was carried out to qualitatively examine the interaction of the MLS and polymer. Samples were prepared in a mixture of epoxy and hardener in order to slice the samples using an ultramicrotome with a diamond knife. The microtomed samples were then examined under a JEOL 2010 FasTEM transmission electron microscope at 120 kV and various magnifications.

#### 3.3. Thermal Analysis

Thermogravimetric analysis (TGA), employing a Hi-Res TGA 2950, was used to determine the amount of nanoparticle in the formulation and thermal stability of the nanocomposite samples. The samples were heated to  $800^\circ\text{C}$  at a rate of  $20^\circ\text{C}/\text{min}$ , using a nitrogen purge.

Differential scanning calorimetry (DSC) was performed with a Perkin-Elmer DSC 7 with a liquid nitrogen cooling accessory. A scan rate of  $20^\circ\text{C}/\text{min}$  was used in the temperature range from  $-100$  to  $100^\circ\text{C}$ . The samples were cycled upon heating and cooling.

Dynamic mechanical analysis (DMA) was performed with a Seiko 210 instrument at a frequency of 1 Hz and a scan rate of  $4^\circ\text{C}/\text{min}$  from  $-140$  to  $90^\circ\text{C}$ . Samples were tested in the tension mode and the following parameters measured: dynamic storage modulus ( $E'$ ), loss modulus ( $E''$ ), and mechanical loss tangent ( $\tan \delta = E''/E'$ ).

#### 3.4. Mechanical Properties

Tensile testing was performed using an Instron instrument with the Series IX 7.50.00 automated materials testing system and interface type 5500. A 50-kg load cell with 250-lb pneumatic grips was used. Film samples (cut with a dog bone die measuring 1/4 in. wide by 4 in. long and with a gauge length of 2 in.) were tested at a crosshead speed of 2 in. per min.

### 3.5. Environmental Degradability

#### 3.5.1. Soil Respirometry Test

Polymer mineralization studies were conducted using a static soil biometer system incorporating elements of both the soil biometer system of Bartha & Pramer<sup>36</sup> and ASTM standard D5988.<sup>37</sup> In general, the test consisted of (i) preparing and characterizing a standard laboratory soil; (ii) exposing representative samples of the nanocomposites to the soil matrix under controlled isothermal and aerobic conditions; (iii) measuring the amounts of  $\text{CO}_2$  produced and  $\text{O}_2$  consumed as a function of time; and (iv) assessing the degree of biodegradability of the nanocomposites by comparing net  $\text{CO}_2$  production/ $\text{O}_2$  consumption from the test materials to that produced from the positive control (i.e., microcrystalline cellulose).

The soil used was a standard soil mix composed of a 1:1:0.1 (w:w:w) mix of potting soil, sand, and composted manure (water holding capacity = 46.4 g of  $\text{H}_2\text{O}/100$  g of soil; pH 7.0; C:N ratio = 17:1). Film samples weighing 660–700 mg (yielding a substrate loading of 5.0 mg of polymer-C  $\text{g}^{-1}$  of soil) were cut into 10 mm  $\times$  10 mm pieces; buried in test reactors containing 75 g of soil at a water content of 60% water-holding capacity (WHC), and incubated in a controlled environment chamber at  $22 \pm 1^\circ\text{C}$  in the dark. Soil water content was maintained at  $55 \pm 5\%$  water-holding capacity by periodically watering the soil with dilute (half strength) Hoagland's solution. Samples of the headspace gas were withdrawn from the reactors at 12–120 h intervals and analyzed for  $\text{CO}_2$  and  $\text{O}_2$  content using a Varian Model CP2003 Micro-GC equipped with Molecular Sieve 5A and Poraplot U columns and dual micro-TCDs (thermal conductivity detectors). Each time the headspace gas was sampled, the systems were aerated by allowing the atmosphere in the bioreactors to exchange and equilibrate with atmospheric air for 5–10 min; at the same time, the soils were hand-mixed to ensure that anaerobic microenvironments did not develop. Daily and cumulative  $\text{CO}_2$  production (total and net) was calculated relative to a control reactor (soil without added polymer). In addition, net mineralization of the cellulose samples was monitored to ensure that the soil could support an actively degrading microbial population throughout the test exposure. All analyses were run in triplicate. Upon completion of the test exposure, soils from the triplicate reactors were combined and stored in a refrigerator at  $4^\circ\text{C}$  until needed for the various toxicity tests (seed germination and root elongation bioassays).

#### 3.5.2. Interpretation of the Biodegradation Data

Biodegradation data were plotted in the form of substrate mineralization versus time curves. A combination of linear (1st degree polynomial; Eq. (1)) and nonlinear (three parameter, single exponential rise to a maximum;

Eq. (2)) regression techniques<sup>38</sup> were used to describe and interpret the net mineralization curves.

$$y = y_0 + bx \quad (1)$$

$$y = y_0 + a(1 - \exp^{-bx}) \quad (2)$$

Model parameters are defined as follows:  $y$  is substrate mineralization expressed as milligrams of  $\text{ThCO}_2$ ;  $y_0$  is the  $y$ -intercept;  $a$  is the amplitude; and  $b$  is the empirical rate constant. Results of the mineralization studies were interpreted using the following response parameters:<sup>39</sup>

- (i) MAX- $\text{CO}_2$ , defined as the maximum amount of  $\text{CO}_2$ -C evolved during mineralization of the test substrate;
- (ii) LAG, defined as the time required for net  $\text{CO}_2$ -C evolution to reach 10% of the MAX- $\text{CO}_2$ ;
- (iii)  $r_{\text{pdp}}$ , defined as average rate of mineralization during the primary degradation phase of the test exposure—calculated as the slope of the linear least-squares regression line plotted between the end of the lag period and the start of the plateau region of the net mineralization curve (i.e., the point where net mineralization =  $2/3$ MAX- $\text{CO}_2$ ), and
- (iv) the relative biodegradation index (RBI), defined as the ratio of cumulative net mineralization of the test sample to cumulative net mineralization of the positive control.

In addition, the time required for mineralization of the nanocomposites to reach 60%  $\text{ThCO}_2$  ( $t_{60}$ ) was calculated from the regression equation that best described the mineralization curve. Based on current ASTM standards, the PBSA/MLS nanocomposites were considered to be 'biodegradable' if they achieved 60%  $\text{ThCO}_2$  during a 180-day test exposure.

The theoretical carbon dioxide ( $\text{ThCO}_2$ ) is the quantity of  $\text{CO}_2$  (in milligrams) calculated to be produced from the measured/calculated carbon content of the test compound when fully mineralized; this also may be expressed as the ratio of the milligrams  $\text{CO}_2$  evolved per milligram of test compound (i.e., as % $\text{ThCO}_2$ ).<sup>40,41</sup>

### 3.6. Phytotoxicity Testing (Seed Germination and Root Elongation)

Upon completion of the respirometry test (i.e., following a 180 day test exposure), any residual pieces of nanocomposite were removed from the test reactors and the soil from each of the three replicate reactors was combined into a single composite sample. Phytotoxicity tests were then carried out using aqueous extracts of the composite soils.

Because of its high sensitivity to phytotoxins, garden cress (*Lepidium sativum*) is an ideal plant for assessing the ecotoxicity of low-level toxins.<sup>42,43</sup> In general, the test consisted of

- (i) obtaining an aqueous extract of each composite soil,
- (ii) incubating cress seeds in contact with the soil:water extracts, and
- (iii) determining seed germination and root elongation.

A subsample of each soil was mixed with deionized (DI) water (50 ml of type II DI water per 40 g of moist soil), incubated at room temperature (ca. 22 °C) for 30 min, filtered through cheesecloth, centrifuged for 15 min at 8000 g and 4 °C, and filter-sterilized through a 0.45- $\mu\text{m}$  membrane filter (Gelman Scientific, Ann Arbor, MI). While maintaining aseptic conditions, a dilution series was prepared (undiluted, 1:4 extract:water, and 1:2 extract:water) from each extract (i.e., for each soil-nanocomposite combination). One milliliter of extract was then pipetted into a 50-mm sterile Petri dish lined with filter paper (Whatman No. 1; 4.25 cm diameter) and 25 cress seeds were placed in each dish. Each dilution was replicated 10 times and the Petri dishes incubated for 24 h at 27 °C in the dark. Seed germination was stopped by adding 1 ml of 50% (v/v) ethanol to each dish. Treatments were evaluated by determining the number of germinated seeds and the length of the root radicle (i.e., the part of a plant that develops into a root).

Percent germination was calculated by dividing the mean germination of each treatment (MGT) by the mean germination in the control (unamended soil) extract (MGC) and multiplying this number by 100. The percent root length was calculated by dividing the mean radicle root length of each treatment (MRLT) by the mean radicle root length of the control (MRLC) and multiplying this number by 100. The phytotoxic effect of degradation products formed during test exposures of the nanocomposites in soil were interpreted using Zucconi's germination index (GI) (Table II), which was calculated by multiplying the percent germination ( $\text{MGT} \div \text{MGC}$ ) by the percent root length ( $\text{MRLT} \div \text{MRLC}$ ).<sup>45</sup>

### 3.7. Statistical Analysis

Exploratory data analysis<sup>44</sup> was used in the initial stage of the statistical analysis to assess the nature of the frequency distribution for each variable and to identify outliers. Outliers (measured value  $\geq$  median value +  $k$ ) were defined using a  $k$  value of 1.5 times the interquartile range and were excluded from the analysis of variance and means separation tests. Analysis of variance (ANOVA) was conducted by using the GLM procedure of CoStat ver. 6.1.<sup>38</sup> However, because the percent data form a binomial distribution, rather than a normal distribution, all such data (e.g., percent mineralization) were transformed using the arcsine transformation prior to analysis of variance.<sup>45</sup> The soil respirometry test employed a one-way completely randomized design (1w-crd) with nanocomposite as the

**Table II.** Garden cress germination index description.

Germination index	Rating (description)
1.0–0.8	No inhibition; little or no phytotoxicity
0.8–0.6	Mild inhibition; minimal phytotoxicity
0.6–0.4	Strong inhibition; phytotoxic
$\leq 0.4$	Severe inhibition; phytotoxic

main factor. Contrast statements included in the ANOVA model were used to assess the significance of differences between predetermined groups of nanocomposites, e.g., the effect of MLS additions to PBSA nanocomposites, the effect of processing speed, and the effects of starch additions to PBSA-MLS nanocomposites. The least significant difference (LSD) test was used to detect significant differences between mean values grouped by nanocomposite composition.

The cress phytotoxicity bioassay was set up as a 2-way completely randomized design (2w-crd) with nanocomposite and dilution as the main factors and seed germination and root length as the variables. The least significant difference (LSD) test was used to detect significant differences between mean values grouped by nanocomposite and dilution factor.

## 4. RESULTS AND DISCUSSION

### 4.1. Morphology

X-ray analysis was conducted to determine the degree of interaction between the MLS and the polymer. A representative X-ray diffraction curve of PBSA powder/MLS 1855, in which the reduction or disappearance of peaks could be indicative of intercalation or exfoliation, is shown in Figure 3. A summary of the  $2\theta$  values and calculated  $d$ -spacings for the various PBSA/MLS nanocomposites is shown in Table III.

X-ray data for PBSA powder/MLS 1330 samples showed a  $d_{001}$ -spacing at approximately 14 Å. The processed mixtures of PBSA powder and the MLS 1330 showed peaks with a slight shift to lower diffraction angles (larger  $d$ -spacing) and large decreases in intensity with higher speed. The intensity of the sample processed at 20 rpm was about half the intensity and was a broader peak than the samples processed at 40 and 60 rpm. The 40 and 60 rpm processed nanocomposites had practically identical X-ray data. This illustrates that the lower screw speeds, having a higher residence time, may promote interaction of the MLS and the polymer, and that the mixing is less efficient at the higher screw speeds. The X-ray data for the PBSA pellet/MLS 1330 follows the same trend as the powder, with the 20 rpm sample having a diffuse broad peak and a lower intensity than the 40 rpm sample.

In the X-ray spectra for the PBSA powder/MLS 1855, Figure 3, the  $d_{001}$ -spacing for the pure MLS occurs at 18 Å. The composite spectra of the 20, 40, and 60 rpm show a disappearance of this  $d_{001}$  peak, indicating possible exfoliation. Again, the samples at 40 and 60 rpm surprisingly show some diffuse peaks, with the 60 rpm sample having more pronounced peaks at approximately 39 and 20 Å. Again, the lower screw speeds show the most interactions from X-ray for the polymer/MLS. The PBSA pellets/MLS 1855 X-ray data demonstrated similar trends with some variation. The 20 rpm data have a peak at

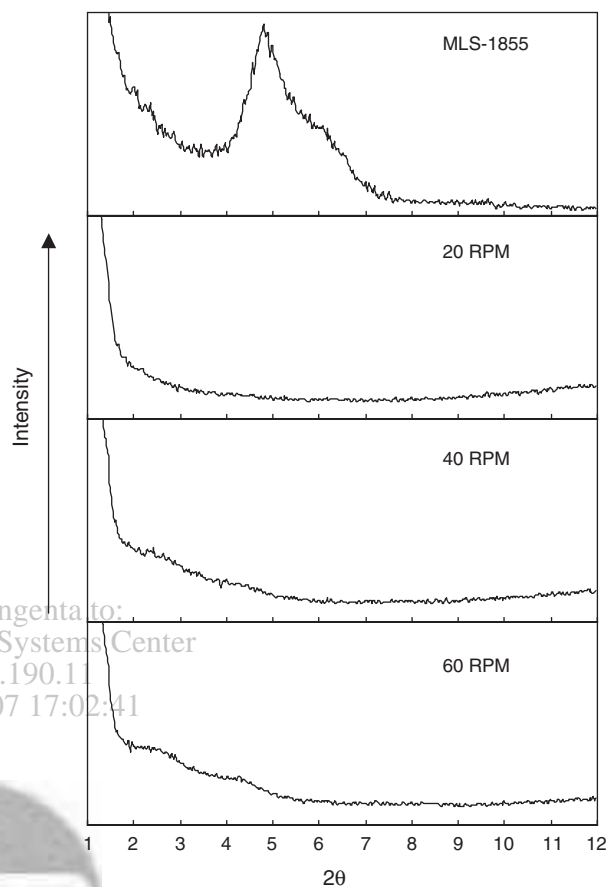


**Fig. 3.** Representative X-ray diffraction curve of PBSA powder/MLS 1855. Reduction/disappearance of peaks indicates possible intercalation or exfoliation.

**Table III.** X-ray data for PBSA/MLS nanocomposites.

Sample	$2\theta$ (deg)			$d$ -spacing Å	
MLS-1330	6.37			13.88	
Powder-1330-20 rpm	6.28			14.07	
Powder-1330-40 rpm	6.28			14.07	
Powder-1330-60 rpm	6.25			14.14	
MLS-1330	6.37			13.88	
Pellet-1330-20 rpm	6.28			14.07	
Pellet-1330-40 rpm	6.28			14.07	
MLS-1855	4.81			18.37	
Pellet-1855-20 rpm	6.43			13.75	
Pellet-1855-40 rpm	6.40*	4.33*	2.25*	13.81	20.41 39.26
Pellet-1855-60 rpm	6.40*	4.45*	2.25*	13.81	19.86 39.26
MLS-1855	4.81			18.37	
Powder-1855-20 rpm	None			None	
Powder-1855-40 rpm	4.48*	2.25*		19.72	39.26
Powder-1855-60 rpm	4.45*	2.25*		19.86	39.26
MLS-1855	4.81			18.37	
Powder-Starch-1855-20 rpm	6.55*	4.30*	2.25*	13.49	20.55 39.26
Powder-Starch-1855-60 rpm	2.71			32.60	
MLS-1856	4.90			18.03	
Pellet-1856-20 rpm	4.55	6.5*		19.42	13.60
Pellet-1856-40 rpm	4.40	6.71*		20.08	13.17

\*Broad, diffuse peaks.

approximately 14 Å, a shift to a lower value from the pure MLS. The 40 and 60 rpm X-ray data are almost identical to each other and to the PBSA powder/MLS 1855 with diffuse peaks at approximately 20.4, 39, and 20 Å.

A PBSA powder/MLS 1855 nanocomposite formulated with starch using a 50/50 masterbatch of the PBSA/starch powder demonstrated a  $d_{001}$ -spacing for the MLS at 18.1 Å and the 20 rpm sample resembled the 60 rpm data for the PBSA/MLS 1855 system without the starch, with diffuse peaks separating at approximately 20, 14, and 39 Å. The 60 rpm data had only one diffuse peak in the region of 32 Å. In the case of the starch/polymer/MLS formulation, the higher screw speed is perhaps essential for mixing all of the components.

The X-ray data for the PBSA pellet/MLS 1856 nanocomposites at 20 and 40 rpm did not vary significantly from the pure MLS-1856. There do not appear to be significant interactions between the nanoparticles and PBSA with  $d$ -spacings of approximately 18, 19, and 20 Å for the MLS-1856, the 20 rpm nanocomposite, and the 40 rpm nanocomposite, respectively.

Overall, the X-ray data demonstrate that some intercalation of galleries of the MLS has occurred with possible

exfoliation of some platelets. The best X-ray data, as far as demonstrating the possibility of the most interaction, is the 20 rpm PBSA powder/MLS 1855. This may be attributed to the differing chemical functionality, where MLS 1855 possesses two functional groups, as well as a long carbon chain, to interact with the polymer, as opposed to MLS 1330, which has only one functional group, and MLS 1856, which although similar in structure to MLS1855, possesses a NH functionality as opposed to the N-CH<sub>3</sub> functionality seen in MLS 1855.

TEM coupled with X-ray diffraction data can confirm the interaction of the polymer and MLS. Figure 4 shows representative TEMs, where the stacking of the MLS layers are seen as alternating dark lines. An example of the PBSA powder/MLS 1330 (3A) processed at 20 rpm is seen in Figures 4(a, b). Clearly, the MLS platelets are not well-dispersed. The 50 nm magnification photograph in Figure 4(a) shows some dispersion of the MLS, while the 10 nm magnification photograph (Fig. 4(b)) displays an intercalated structure. The PBSA powder/starch/1855 sample (6A) at 20 rpm (Fig. 4(c)) shows the MLS platelets in a variety of size and shapes. Figure 4(d) shows more of an intercalated structure for this system. Figures 4(e, f)

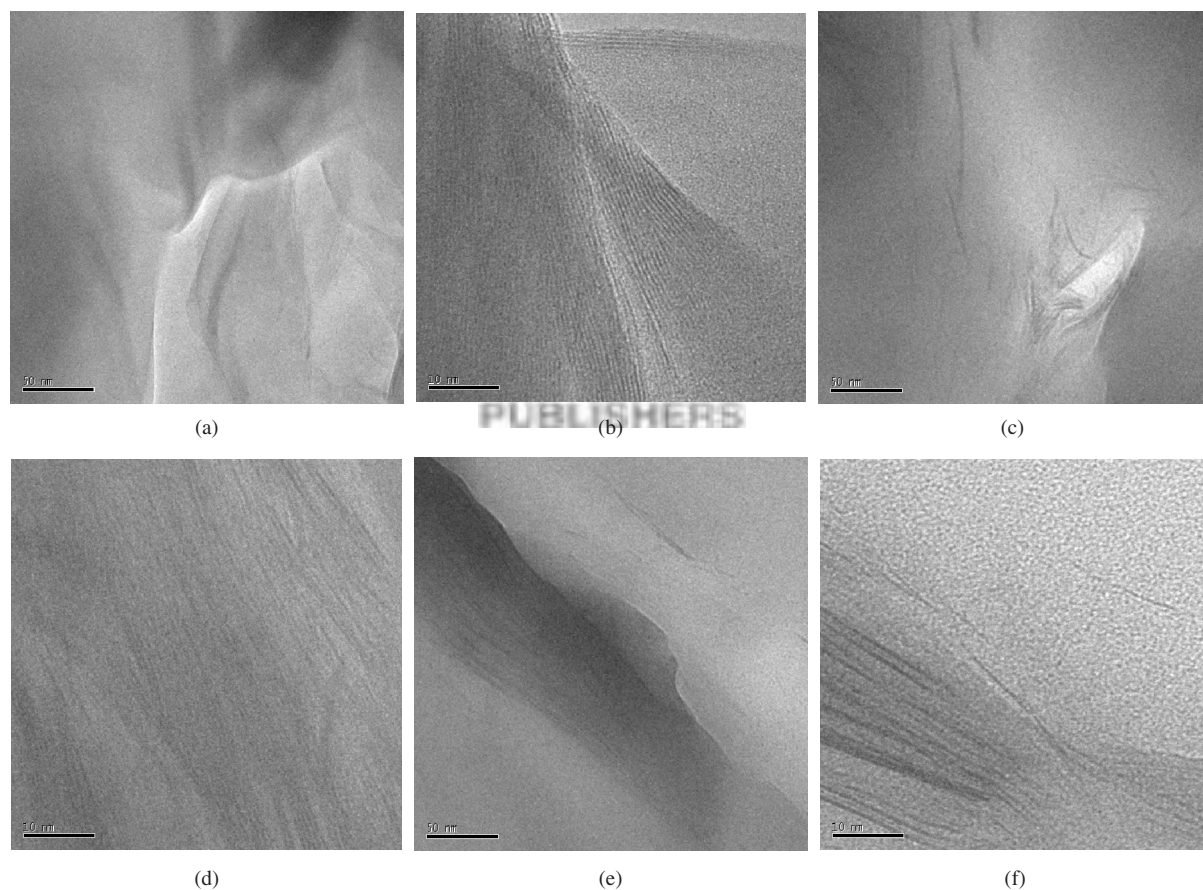


**Fig. 4.** TEMs of PBSA/MLS nanocomposites: (a) 3A PBSA (powder)/MLS 1330, 20 rpm, magnification 50 nm; (b) 3A PBSA (powder)/MLS 1330, 20 rpm, magnification 10 nm; (c) 6A PBSA (powder)/Starch/MLS 1855, 20 rpm, magnification 50 nm; (d) 6A PBSA (powder)/Starch/MLS 1855, 20 rpm, magnification 10 nm; (e) 7A PBSA (pellet)/MLS 1856, 20 rpm, magnification 50 nm; (f) 7A PBSA (pellet)/MLS 1856, 20 rpm, magnification 10 nm.

are images of the 7A, PBSA pellet/MLS 1856 at the same magnifications. Similar photographs are seen for these samples as the other samples, indicating again some possible intercalation in the different formulations.

## 4.2. TGA

TGA was performed to determine the amount of inorganic residue in the nanocomposite and to evaluate any changes in thermal stability. All formulations incorporated 5% by weight of MLS into the PBSA; however, there maybe some inhomogeneous mixing causing some variation in the residue results from TGA. The percent residue ranged from a low of 1.3% for the sample PBSA powder/MLS 1855 20 rpm (5A) to a high of 6.9% for sample PBSA powder/starch/MLS 1855 60 rpm (6C) as displayed in Table I. However, the majority of samples were in the 3.2–4.4% range. There does not appear to be any relationship between the PBSA form (powder versus pellet) and the amount of residue.

For the thermal stability, there was no significant change to the thermal stability in any formulation in comparison to the pure PBSA. The shape of the curves was similar to that of the existing PBSA and there were no significant shifts in the weight loss curve for any formulation. Other intercalated nanocomposites systems studied have shown significant shifts in thermal stability ranging from 9 °C to 80 °C.<sup>46,47</sup>

## 4.3. DSC

Table IV displays the melting temperature ( $T_m$ ) and enthalpy values for the different formulations for second heat data. For the MLS 1330 formulations, the values do not vary significantly despite the screw speed or powder versus pellet preparation. The  $T_m$  decreases a few degrees below the pure PBSA value and the enthalpy also

**Table IV.** DSC data for PBSA/MLS nanocomposites.

ID	Sample	$T_m$ (°C)*	$\Delta H$ (J/g)
1A	Pure PBSA 3001: 10 rpm	94.5	41.4
2A	PBSA (pellet)/MLS 1330: 20 rpm	94.0	33.6
2C	PBSA (pellet)/MLS 1330: 40 rpm	91.1	39.5
3A	PBSA (powder)/MLS 1330: 20 rpm	93.5	31.3
3B	PBSA (powder)/MLS 1330: 40 rpm	92.3	31.7
3C	PBSA (powder)/MLS 1330: 60 rpm	92.1	33.5
4B	PBSA (pellet)/MLS 1855: 20 rpm	93.7	30.9
4C	PBSA (pellet)/MLS 1855: 40 rpm	89.8	35.4
4D	PBSA (pellet)/MLS 1855: 60 rpm	92.1	36.0
5A	PBSA (powder)/MLS 1855: 20 rpm	84.5	32.7
5B	PBSA (powder)/MLS 1855: 40 rpm	88.5	34.9
5D	PBSA (powder)/MLS 1855: 60 rpm	90.7	40.6
6A	PBSA (powder)/MLS 1855/starch: 20 rpm	92.9	32.5
6C	PBSA (powder)/MLS 1855/starch: 60 rpm	93.0	24.5
7A	PBSA (pellet)/MLS 1856: 20 rpm	93.1	34.6
7C	PBSA (pellet)/MLS 1856: 60 rpm	93.1	37.5

\*Determined from second heat DSC data.

decreases slightly, indicating the MLS is not acting as a nucleating agent. The PBSA/MLS 1855 pellet and powder samples at 40 rpm behave similarly to each other. The  $T_m$  decreases approximately 5 °C, while the enthalpy drops by 6 J/g for the nanocomposite samples in comparison to the pure PBSA. These differences in the thermal properties indicate polymer and nanoparticle interactions as did the X-ray data where  $d$ -spacing changed with the addition of MLS 1855. The 60 rpm samples of both powder and pellet have values similar to the pure PBSA. The sample with starch at 60 rpm has a lower enthalpy value than pure PBSA, indicating less crystallinity.

The PBSA/MLS 1856 samples all had similar values to the pure PBSA, independent of the screw speed. The DSC in general shows the glass transition temperature ( $T_g$ ) as a small transition at approximately -30 °C and the melting peak for the PBSA at 94 °C. The shapes of the DSC curves for all samples were very similar. The melting peaks are almost identical with the enthalpy values also comparable. The melt peaks are broad and  $T_g$  transition does not indicate anything about the MLS/polymer interactions. There is no change in the DSC curves using the pellet or powder form of PBSA or for different screw speeds. As previously mentioned, an exception is the DSC trace for the sample with starch where the smaller melting peak exists.

## 4.4. DMA

Representative DMA data ( $E'$  versus temperature and  $\tan \delta$  versus temperature) are shown in Figures 5(a, b). The DMA data have a broad  $\tan \delta$  peak in the range of -70 to -20 °C with a peak maximum at approximately -45 °C which corresponds to the  $T_g$  of the PBSA. There were no significant  $T_g$  changes or modulus shifts in the DMA data for the PBSA/MLS 1330 or 1856 nanocomposites. The PBSA pellet/MLS 1855 had only slight shifts in the data, while the PBSA powder/MLS 1855 had more significant changes throughout the temperature range of the experiment. The  $E'$  data for the PBSA powder/MLS 1855 formulation without starch in Figure 5(a) does show that the 20 and 60 rpm samples are similar to the pure PBSA with the 20 rpm data being lower throughout the entire temperature range, and the 60 rpm data exhibits higher values for the storage modulus at temperatures above the  $T_g$ . The 20 rpm sample containing starch has considerably less rigidity than pure PBSA over the entire temperature range, while the 60 rpm starch sample demonstrates an increase in rigidity, exceeding that observed for the 60 rpm sample without starch. Although the X-ray data for the 20 rpm PBSA powder/MLS 1855 indicate the most promise for exfoliated/interacted morphology, DMA data do not show any enhanced rigidity. This sample also contains the lowest amount of 1855, so this may also be a factor contributing to these dynamic mechanical properties. The 60 rpm starch sample does show a different X-ray pattern than the 20 rpm sample, and the DMA data are also different. In a

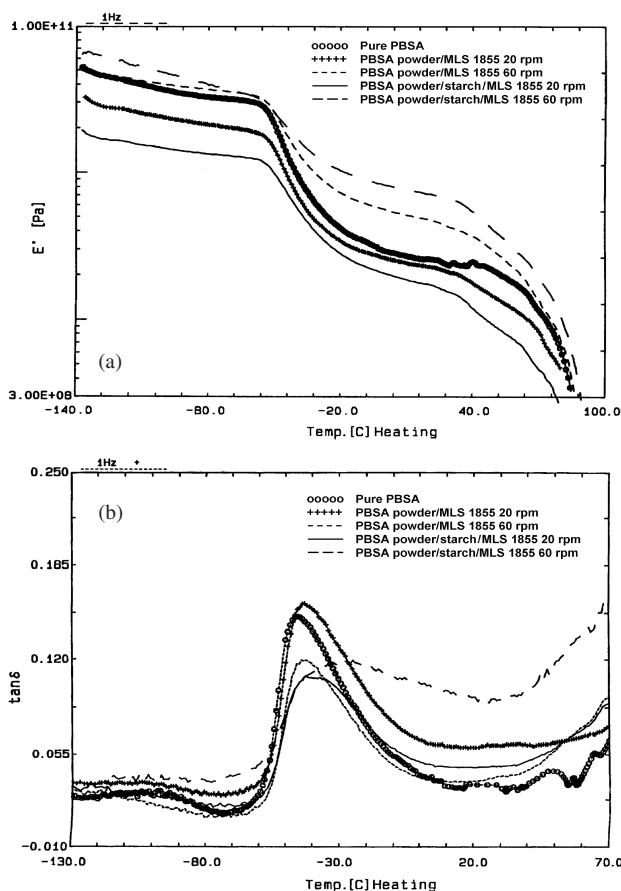


**Fig. 5.** DMA data of PBSA powder/MLS 1855 samples. (a)  $E'$  versus temperature: (o) pure PBSA, (+) PBSA powder/MLS 1855 20 rpm, (---) PBSA powder/MLS 1855 60 rpm, (—) PBSA powder/starch/MLS 1855 20 rpm, (---) PBSA powder/starch/MLS 1855 60 rpm. (b)  $\tan \delta$  versus temperature: (o) pure PBSA, (+) PBSA powder/MLS 1855 20 rpm, (---) PBSA powder/MLS 1855 60 rpm, (—) PBSA powder/starch/MLS 1855 20 rpm, (---) PBSA powder/starch/MLS 1855 60 rpm.

previous study with PBSA and starch, higher values of  $E'$  were observed with 20% and 30% starch in PBSA blown films in comparison to pure PBSA blown film.<sup>13</sup>

The  $\tan \delta$  data for PBSA powder/MLS 1855 at 20 rpm has a slight shift of the peak maximum ( $T_g$ ) from the pure PBSA with also slightly broader peak. The 60 rpm data has the same  $T_g$  as the pure PBSA. The sample with the starch extruded at 20 rpm has a broader peak with a shift of the transition to slightly higher temperature. The  $\tan \delta$  peak for the 60 rpm starch data is a very broad curve and the peak maximum is shifted to high temperatures. There are no transitions from starch visible in the DMA data. The  $T_g$  of the starch is expected to be above the melting of the PBSA.

#### 4.5. Mechanical

The stress-strain behavior of PBSA 3001 and PBSA/MLS are similar to that of polypropylene; where the polymer begins to neck after a yield point. Overall, the mechanical

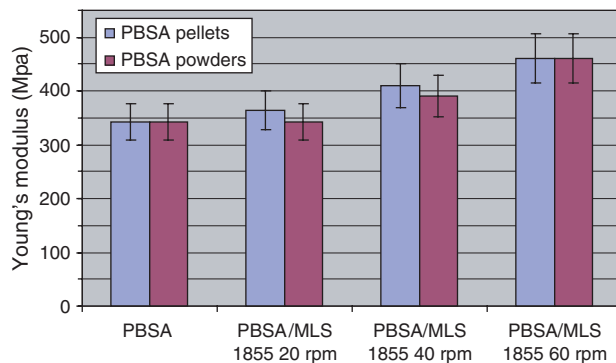


**Fig. 6.** Representative Young's modulus values for PBSA/MLS nanocomposites.

properties do not improve significantly with the addition of any of the MLSs. In fact, as expected, the elongation and toughness decrease with the addition of MLS. The Young's modulus does improve, but not as much as with other intercalated and/or exfoliated nanocomposites reported in the literature.<sup>11,46</sup>

For Young's modulus values, the pure PBSA is at 342 MPa. For the PBSA pellet/MLS 1330 the modulus range was 340–334 MPa and slightly higher for the PBSA powder/MLS 1330 at 362–368 MPa. But within experimental error, the samples are not significantly different from the PBSA. The PBSA pellet/MLS 1855 were slightly higher from 369 to 456 MPa and the highest values were for the sample processed at 60 rpm. The PBSA powder/MLS 1855 had values for 20 and 40 rpm at 340 and 390 MPa, respectively. The samples containing PBSA powder/starch and MLS/1855 were all about 500 MPa, regardless of the screw speed. The Young's modulus data for the samples containing MLS 1855 are summarized in Figure 6.

The PBSA pellets/MLS 1855 does have the Young's modulus change as a function of screw speed with 60 rpm showing the highest improvement, but this nanocomposite also has the largest decrease in elongation, 4.5 times less than the pure PBSA, and also a toughness of 5 times lower than that of PBSA. These data indicate that the screw speed does influence the interaction of the MLS with the PBSA. This is consistent with the intercalation observed in the X-ray data.

However, the PBSA/MLS/starch sample has a Young's modulus that reaches as high as 507 MPa for the 60 rpm sample and still maintains its tensile strength. The extent of mixing of the starch and nanoparticles at the high screw speed (60 rpm) versus the lower screw speed may play a role in these mechanical results. The lower screw speed may have not been sufficient mixing for the starch and this may create partially melted starch agglomerates in the film which may influence the mechanical properties. The toughness is maintained and the elongation has similar properties to the pure PBSA with decreases as the screw

speed increases. In the previous study on blown film samples containing PBSA and starch, a 30% starch formulation also had an increase of about 200 MPa as with the PBSA/MLS sample.<sup>13</sup> However, the other mechanical properties all decreased with increasing MLS content, with elongation, tensile strength, and toughness values all at least halved in comparison to the pure PBSA film. In the previous study, no films could be processed after 30% starch. Processing was difficult with extremely brittle films as the product. With this MLS we have been able to process higher amounts of starch with the PBSA and achieve some stable mechanical properties relative to the homopolymer, yet at a screw speed of 60 rpm, a brittle film was obtained.

## 4.6. Environmental Degradability

### 4.6.1. Soil Respirometry Test

Results obtained for the unamended soil and the positive control (i.e., the soil amended with cellulose powder) during a 180-day soil test exposure are presented in Figure 7(A). In the control soil, CO<sub>2</sub> production resulted from mineralization of the soil organic matter. Mineralization of this organic matter proceeded in a linear fashion at a rate of about 0.34 mg of CO<sub>2</sub>-C day<sup>-1</sup> throughout the 180-day test exposure. Mineralization of the positive control (cellulose) proceeded slowly at first (with a lag

period of about 6 days) but then increased rapidly from about day 7 to day 21 (Fig. 7(A)). After day 21, net CO<sub>2</sub> production continued to increase for another three weeks—though at a much slower rate—before reaching a plateau at about day 45. Because the time required to achieve 60% net mineralization (ca. 17 days) occurred within a “14-day window following the lag period,” the positive control is considered ‘readily biodegradable’ (as defined by EPA method 835.3110: *Ready Biodegradability*).<sup>40</sup>

Total net mineralization of the positive control (i.e., total net CO<sub>2</sub>-C production from the cellulose-amended soil) exceeded 100%, which is indicative of a ‘priming effect.’<sup>48</sup> That is, addition of a readily biodegradable substrate to the soil results in an increase in both the size and activity of the indigenous microbial population. This, in turn, results in enhanced mineralization of the soil organic matter as the added substrate (in this case, cellulose powder) is depleted—yielding amounts of *net* CO<sub>2</sub>-C that may exceed 100% of the added substrate-C.

Net mineralization curves for the pure PBSA films are presented in Figure 7(B). Cumulative net mineralization of the films averaged about 62% upon completion of the 180-day test exposure. The *t*<sub>60</sub> for these films (i.e., the time required for mineralization of the films to reach 60% ThCO<sub>2</sub>) was between 170 and 180 days; hence, the PBSA was not considered ‘readily biodegradable’ material. However, the PBSA did reach the 60% net mineralization threshold for classification as biodegradable (compostable) materials within the time limit (180 days) defined by the ASTM.

Net mineralization curves for the various PBSA-MLS nanocomposites are presented in Figures 8–11. In general, the mineralization curves exhibited a biphasic pattern with a plateau (defined as a ‘flattening’ of the curve) occurring between day 63 and day 98. This was followed by a relatively short period of rapid mineralization and a near-linear increase in cumulative net CO<sub>2</sub>-C from day 119 to day 180. Increased rates of net mineralization during the period from day 98 to day 119 were preceded by the addition of dilute nutrient solution used to adjust the soil water content to 55 ± 5% WHC. Thus, decreased mineralization of the nanocomposites in the plateau region most likely reflects the impact of water/nutrient stress on the community of polymer-degrading microorganisms in the soil. Nutrient solution was added to the soils again on day 168; however, this had no consistent effect on net CO<sub>2</sub>-C production, suggesting that mineralization of the nanocomposites was not limited by water or nutrient stress during the latter phase of the test exposure.

Despite the biphasic pattern, linear regression techniques employing a first-order polynomial model provided a relatively good description of the net mineralization curves. Indeed, starting from the end of the lag period and ending at day 180, the linear model yielded an excellent fit to the experimental data ( $R^2 \geq 0.980^{***}$ ), with calculated

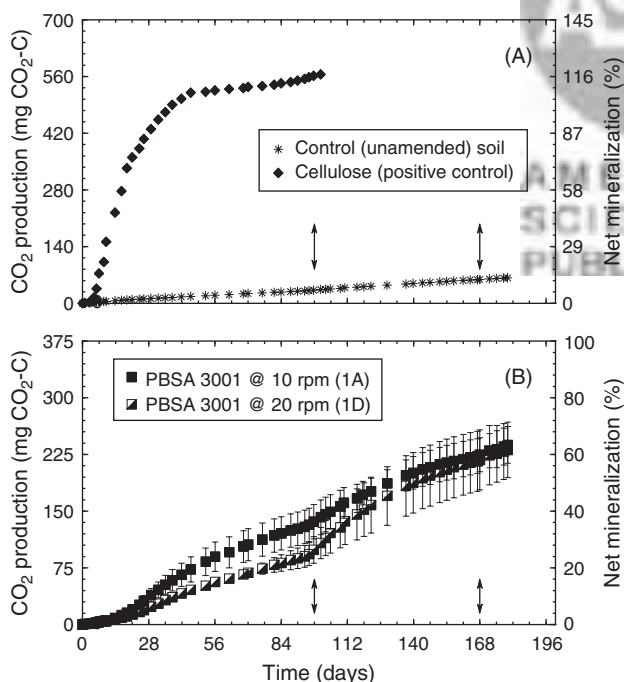


**Fig. 7.** (A) Carbon dioxide produced by the control (unamended) soil and soil amended with cellulose powder (positive control) at 22 °C and 55 ± 5% water-holding capacity (WHC). (B) Net mineralization of PBSA 3001 films in soil at 22 °C and 55 ± 5% water-holding capacity. *Note:* Arrows indicate days on which the water content of the soil was adjusted to ca. 60% WHC using a dilute nutrient solution.

**Table V.** Mineralization of the PBSA-MLS nanocomposite films and positive control (cellulose) during a 180-day test exposure in soil at  $22 \pm 1$  °C and a moisture content of  $55 \pm 5\%$  WHC.

Polymer substrate		Mineralization						
ID	Description	Lag <sup>a</sup> (days)	Max-CO <sub>2</sub> C <sup>b</sup> (mg)	ThCO <sub>2</sub> (%)	RBI <sup>c</sup>	RQ <sup>d</sup>	r <sub>pdp</sub> <sup>e</sup> (mg of C day <sup>-1</sup> )	t <sub>60</sub> <sup>f</sup> (days)
Cell	Cellulose powder	6	565 ± 49.1	116 ± 10	3.46	21.6 ± 2.1	17	
1A	PBSA 3001: 10 rpm	25	240 ± 24.3	63 ± 7	0.54	2.55	1.31 ± 0.03	169
1D	PBSA 3001: 20 rpm	35	231 ± 36.6	61 ± 10	0.53	2.67	1.50 ± 0.07	176
2C	PBSA (pellet)/MLS 1330: 40 rpm	29	252 ± 27.7	67 ± 7	0.58	2.66	1.47 ± 0.06	152
3A	PBSA (powder)/MLS 1330: 20 rpm	26	238 ± 33.0	63 ± 9	0.54	2.31	1.33 ± 0.05	161
3B	PBSA (powder)/MLS 1330: 40 rpm	26	267 ± 22.8	71 ± 5	0.61	2.56	1.55 ± 0.05	140
3C	PBSA (powder)/MLS 1330: 60 rpm	30	221 ± 25.3	58 ± 6	0.50	2.44	1.28 ± 0.03	176
4B	PBSA (pellet)/MLS 1855: 20 rpm	27	288 ± 37.2	76 ± 9	0.66	2.63	2.03 ± 0.08	124
4C	PBSA (pellet)/MLS 1855: 40 rpm	27	244 ± 68.0	64 ± 18	0.55	2.62	1.54 ± 0.14	157
5A	PBSA (powder)/MLS 1855: 20 rpm	30	260 ± 41.1	69 ± 11	0.59	2.74	1.61 ± 0.06	148
5D	PBSA (powder)/MLS 1855: 60 rpm	39	231 ± 27.0	61 ± 6	0.53	2.55	1.51 ± 0.05	174
6A	PBSA (powder)/MLS 1855/Starch: 20 rpm	33	227 ± 8.2	60 ± 2	0.52	2.46	1.30 ± 0.03	173
6C	PBSA (powder)/MLS 1855/Starch: 60 rpm	15	194 ± 36.4	51 ± 10	0.44	2.27	3.40 ± 0.15	184
7A	PBSA (pellet)/MLS 1856: 20 rpm	33	225 ± 11.5	60 ± 2	0.52	2.47	1.34 ± 0.05	173
7C	PBSA (pellet)/MLS 1856: 40 rpm	36	171 ± 24.2	46 ± 6	0.40	2.13	1.01 ± 0.03	236

<sup>a</sup>Time required for net mineralization to reach 10% of the MAX-CO<sub>2</sub>. Note: In cases where the net mineralization curve did not reach a plateau, the Lag was defined as the time required for net CO<sub>2</sub>-C evolution to reach 5% ThCO<sub>2</sub>.

<sup>b</sup>The maximum amount of CO<sub>2</sub>-C evolved during the 180-day test exposure.

<sup>c</sup>Relative biodegradation index = (percent mineralization of the test sample ÷ percent mineralization of the positive control); positive control = cellulose.

<sup>d</sup>Respiratory quotient; mmole of CO<sub>2</sub> produced per mmol of O<sub>2</sub> consumed.

<sup>e</sup>Average rate of mineralization during the primary degradation phase: defined as the slope of the linear least-squares regression line plotted between the end of the lag period and start of the plateau region (i.e., the point where net mineralization = two-thirds MAX-CO<sub>2</sub>). Note: In cases where the net mineralization curve did not reach a plateau, the r<sub>pdp</sub> was calculated for the period from the end of the lag period to the end of the test exposure.

<sup>f</sup>Time required for substrate mineralization to reach 60% ThCO<sub>2</sub>.

mineralization constants ( $r_{pdp}$ ) ranging from 1.01 to 3.40 mg CO<sub>2</sub>-C day<sup>-1</sup> (Table V). Whereas mineralization constants for the PBSA-MLS nanocomposites were about an order of magnitude lower than that for cellulose (ca. 22 mg of CO<sub>2</sub>-C day<sup>-1</sup>), they were 2.5- to 5-times greater than that of the soil organic matter (0.34 mg of CO<sub>2</sub>-C day<sup>-1</sup>). In addition, mineralization of the nanocomposites was characterized by RQ values ( $2.50 \pm 0.17$  (mmol of CO<sub>2</sub>)/(mmol of O<sub>2</sub>)<sup>-1</sup>) that were significantly lower than that of the positive control ( $3.46$  (mmol of CO<sub>2</sub>)/(mmol of O<sub>2</sub>)<sup>-1</sup>) but significantly greater than that of the soil organic matter ( $1.88$  (mmol of CO<sub>2</sub>)/(mmol of O<sub>2</sub>)<sup>-1</sup>). Taken together, these results indicate that the nanocomposites are inherently (though somewhat slowly) biodegradable in soil. Total net mineralization of the PBSA/MLS nanocomposites averaged about  $62 \pm 8\%$  ThCO<sub>2</sub> with an average  $t_{60}$  of about 168 days.

Although the impact of incorporating MLS into PBSA-based nanocomposites was confounded by factors such as the form of PBSA used (i.e., powder versus pellet), the type of MLS added, processing speed, and the addition of other fillers (i.e., starch), the analysis of variance revealed that the overall biodegradability (i.e., rate, extent, and ease of degradation) of the PBSA was significantly affected by the addition of the MLS. Indeed, all other factors being equal, the incorporation of MLS into the PBSA matrix yielded nanocomposites with significantly improved bioenvironmental degradability (Fig. 8; Table V). For example, mineralization curves for nanocomposites prepared from

PBSA powder and incorporating MLS 1330 (3A) and 1855 (5A), all prepared at a processing speed of 20 rpm, were characterized by linear rate constants ( $1.58 \pm 0.03$  mg of CO<sub>2</sub>-C day<sup>-1</sup>) and total amounts of net mineralization ( $70 \pm 1\%$  ThCO<sub>2</sub>) that were greater than those obtained for the pure PBSA powder (1D). Moreover, the PBSA-MLS nanocomposites reached the 60% ThCO<sub>2</sub> threshold an average of 25 days sooner than the pure PBSA samples. The PBSA/MLS 1855 generally outperformed the PBSA/MLS 1330 in the soil respirometry tests

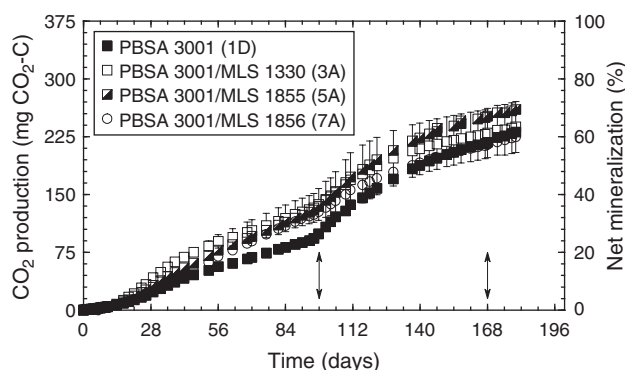


**Fig. 8.** Effect of MLS additions on the net mineralization of PBSA 3001 films in soil at 22 °C and  $55 \pm 5\%$  water-holding capacity. All nanocomposites contained 5% (w/w) MLS and were processed using a conical twin-screw extruder at 20 rpm. Note: Arrows indicate days on which the water content of the soil was adjusted to ca. 60% WHC using a dilute nutrient solution.

**Table VI.** Summary statistics for selected contrasts.

Contrast	Description	Mineralization <sup>†</sup> (%)	Linear rate constant <sup>†</sup> (mg of CO <sub>2</sub> -C day <sup>-1</sup> )	RQ (mmol of CO <sub>2</sub> produced per mmol of O <sub>2</sub> consumed) <sup>†</sup>
1A versus 1D	PBSA (powder) versus PBSA (pellet)	ns	17.00***	6.22*
1D versus 3A + 5A	Effect of MLS additions to PBSA @ 20 rpm	ns	ns	16.80***
3A + 3C versus 5A + 5D	PBSA-MLS 1330 versus PBSA-MLS 1855	ns	61.23***	61.21***
3A + 3B versus 7A + 7C	PBSA-MLS 1330 versus PBSA-MLS 1856	7.35*	66.13***	15.30***
3A versus 3B + 3C	Effect of processing speed (PBSA-MLS 1330)	ns	4.54*	20.21***
3A + 4B + 7A versus 3B + 4C + 7C	Effect of processing speed: 20 rpm versus 40 rpm	ns	21.49***	ns
3A + 5A + 6A versus 3C + 5D + 6C	Effect of processing speed: 20 rpm versus 60 rpm	ns	60.33***	8.75**
5A + 5D versus 6A + 6C	Effect of starch addition to PBSA-MLS 1855	ns	230.74***	65.83***
4B + 4C versus 3A + 3B + 7A + 7C	PBSA-1855 versus PBSA-MLS-1330 versus PBSA MLS-1856	6.95*	235.58***	74.23***

<sup>†</sup>F statistic calculated from the analysis of variance (ANOVA). The symbols \*, \*\*, and \*\*\* denote significant differences at the  $P \leq 0.05$ ,  $P \leq 0.01$ , and  $P \leq 0.001$  levels of probability, respectively.

(Figs. 9(A, B)). That is, whereas there were no significant differences in total net mineralization ( $F = 0.74$  ns), rate constants for the PBSA-MLS 1855 nanocomposites were significantly greater ( $F = 61.23$ \*\*\*) than those of the PBSA-MLS 1330 nanocomposites (Table VI). Likewise, RQ values for the PBSA-MLS 1855 nanocomposites were significantly greater ( $F = 61.21$ \*\*\*) than those for the PBSA/MLS 1330 nanocomposites, suggesting that less energy was required to degrade the PBSA/MLS 1855. These results suggest that MLS 1855 possesses one or more characteristics that enhance the bioenvironmental degradability of PBSA-based nanocomposites.

On the other hand, the mineralization characteristics of the PBSA-MLS 1856 nanocomposites (Fig. 9(C); Table V) were significantly different from those of either the PBSA-MLS 1330 or PBSA-MLS 1855 nanocomposites. This was particularly true of the PBSA/MLS 1856 that was processed at the higher speed (i.e., 40 rpm, sample no. 7C). Indeed, this nanocomposite yielded the least amount of total net CO<sub>2</sub>-C (171 mg; 46% net mineralization) and exhibited the lowest rate constant (1.01 mg CO<sub>2</sub>-C d<sup>-1</sup>) and respiratory quotient (2.13 (mmol of CO<sub>2</sub>)(mmol of O<sub>2</sub>)<sup>-1</sup>) of all the PBSA-based nanocomposites. These results contradict those obtained with the PBSA-MLS 1330 nanocomposites (see Fig. 9(A)) and suggest that high-speed mixing of the PBSA pellets and MLS 1856 produces a nanocomposite with (structural) properties that reduce its inherent biodegradability.

Despite the confounding effects imposed by variations in composition of the nanocomposites, the analysis of variance revealed that varying the processing speed had a significant impact on both the rate (defined by the linear rate constant) and ease (using the respiratory quotient as an indicator) of degradation of the PBSA-MLS nanocomposites (Tables V and VI). In general, mineralization curves for the nanocomposites processed at 60 rpm were characterized by longer lag periods, slower mineralization kinetics (requiring longer times to achieve the

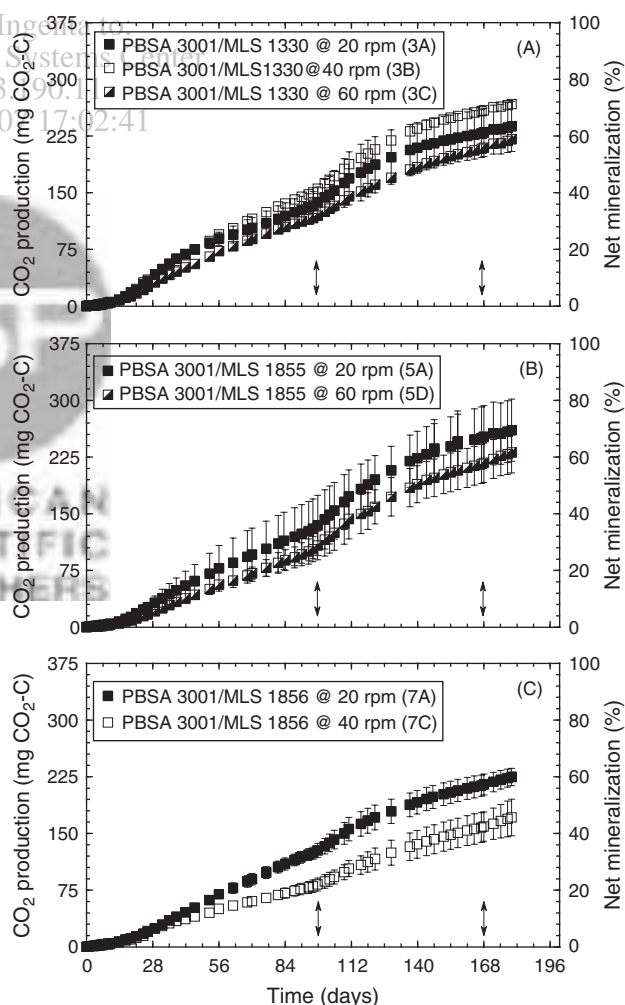


**Fig. 9.** Effect of processing speed on the net mineralization of PBSA/MLS films in soil at 22 °C and 55 ± 5% water-holding capacity. All nanocomposites contained 5% (w/w) MLS and were processed using a conical twin-screw extruder. *Note:* Arrows indicate days on which the water content of the soil was adjusted to ca. 60% WHC using a dilute nutrient solution.

60% ThCO<sub>2</sub> threshold for biodegradable polymers), and lower respiratory quotients than the nanocomposites processed at slower speeds. As well, total net mineralization of the nanocomposites processed at 60 rpm was generally lower than for the other nanocomposites, though the difference was significant only for the PBSA-MLS 1856 nanocomposites.

Starches are readily biodegradable; thus, by incorporating a starch into a nanocomposite, it is expected that the biodegradability of the nanocomposite will be improved. Indeed, extrusion blown films incorporating corn starch in a PBSA 3001 matrix (at starch contents ranging from 5% to 30%) have been shown to degrade (mineralize) more rapidly and to a greater extent than films of the homopolymer alone.<sup>13</sup> In the present study, however, we observed that the incorporation of starch into the PBSA-MLS 1855 nanocomposite had no significant impact on net mineralization of the nanocomposite (Fig. 10; Tables V and VI). The starch-filled nanocomposite processed at 20 rpm (Fig. 10(A)) exhibited a slower rate of mineralization and lower respiratory quotient than the PBSA-MLS 1855 nanocomposite (Fig. 10(A); Table V). This suggests that the starch was compartmentalized within the nanocomposite in a way that reduced its susceptibility to microbial attack. Similar results have been observed with starch-polyethylene blends.<sup>39</sup>

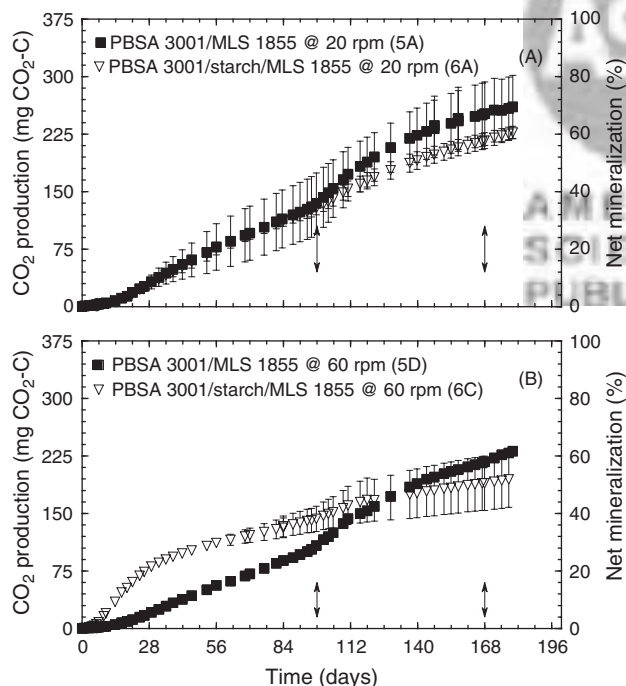


**Fig. 10.** Effect of starch additions on the net mineralization of PBSA/MLS 1855 films in soil at 22 °C and 55 ± 5% water-holding capacity. All nanocomposites contained 5% (w/w) MLS and were processed using a conical twin-screw extruder. (A) Films processed at 20 rpm; (B) films processed at 60 rpm. *Note:* Arrows indicate days on which the water content of the soil was adjusted to ca. 60% WHC using a dilute nutrient solution.

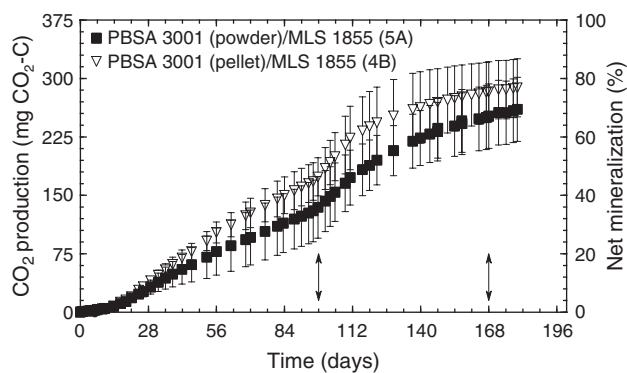


**Fig. 11.** Net mineralization of PBSA/MLS 1855 films in soil at 22 °C and 55 ± 5% water-holding capacity. All nanocomposites contained 5% (w/w) MLS and were processed using a conical twin-screw extruder at 20 rpm. (A) PBSA processed in powder form; (B) PBSA processed in pellet form. *Note:* Arrows indicate days on which the water content of the soil was adjusted to ca. 60% WHC using a dilute nutrient solution.

Conversely, net mineralization curves for the PBSA/MLS 1855/starch nanocomposite processed at 60 rpm (6C) exhibited a shape that is more characteristic of a material containing a readily biodegradable component (Fig. 10(B)). That is, following a relatively short lag period, there was a rapid increase in net mineralization (with a linear rate constant of about 3.40 mg of CO<sub>2</sub>-C day<sup>-1</sup>) as the readily degradable component (starch) was mineralized. This was followed by an extended period during which CO<sub>2</sub> evolution slowed to a near-constant rate (with a linear rate constant of about 0.83 mg of CO<sub>2</sub>-C day<sup>-1</sup>) as the more slowly biodegradable component (PBSA) was mineralized. These results certainly suggest that under the right conditions, the incorporation of starch into PBSA-MLS nanocomposites may result in materials with enhanced biodegradation characteristics.

It was thought that differences in the environmental performance of the PBSA/MLS 1856 and PBSA/MLS 1330 or MLS 1855 nanocomposites (Fig. 9) may reflect differences in the form of the PBSA used to prepare the nanocomposites. That is, whereas PBSA pellets were mixed with the MLS 1856, powdered PBSA was used to prepare the MLS 1330 and 1855 materials. However, a biodegradation study conducted with powdered and pelleted PBSA mixed with MLS 1855 (see Fig. 11) found that the nanocomposite prepared from the PBSA pellets exhibited better biodegradability characteristics (Table V) than the nanocomposite prepared from powdered PBSA. Although the reasons for this are still unclear, these results are in keeping with the general observation that the PBSA/MLS 1855 nanocomposites generally outperformed the PBSA/MLS 1856 and PBSA/MLS 1330 nanocomposites in terms of overall bioenvironmental degradability.

#### 4.7. Phytotoxicity

Early plant growth is usually rapid; hence, seedlings generally exhibit high levels of metabolic activity. Consequently,

the early stages in a plant's development are often more sensitive to the presence of potentially toxic chemicals than are the later stages of plant growth.<sup>48</sup> To take advantage of this, seed germination and root elongation assays have been developed as indicators of the presence of phytotoxic compounds in soils and composts. In this study, the garden cress bioassay was used to determine whether or not phytotoxins were produced during biodegradation of the nanocomposites under soil burial conditions.

Given the chemical nature of the PBSA-based nanocomposites, the only byproducts of the mineralization process should be CO<sub>2</sub> and H<sub>2</sub>O. Thus, any phytotoxic effects would have to be associated with microbial metabolites produced during the biodegradation process. Bioassay results for the cress phytotoxicity with the ANOVA analysis revealed that biodegradation of the nanocomposites had essentially no impact on either seed germination or radicle length (data not shown). Consequently, there were only very small differences in the germination indices, and there was no evidence of a phytotoxic effect following biodegradation of the PBSA/MLS materials.

## 5. CONCLUSION

PBSA/MLS nanocomposite formulations were prepared using either powder or pellets of PBSA and different modified MLS by melt extrusion and characterized for morphological, thermal, and mechanical properties. X-ray and TEM showed varying degrees of intercalated systems with MLS-1855 samples showing more changes in the X-ray *d*-spacing. The thermal analysis showed that the thermal stability did not improve in any formulation and overall the *T<sub>g</sub>*, *T<sub>m</sub>*, and enthalpy transitions did not significantly change for the MLS 1330 and 1856 systems, but there was some variation in thermal transitions for the MLS 1855 samples. The DMA did show some improved *E'* values as a function of temperature for the MLS 1855 samples. The mechanical properties overall did not improve significantly.

The samples were extensively evaluated for biodegradation rates. Standardized (ASTM equivalent) tests were conducted to assess the environmental degradability and ecotoxicity of PBSA-MLS nanocomposites under soil burial conditions. Whereas total net mineralization of the PBSA was generally unaffected by the incorporation of MLS, the ease of mineralization generally increased with the addition of the MLS. That is, the PBSA/MLS materials generally degraded at a faster rate than the pure PBSA. This was particularly true for MLS 1855. The environmental degradability of the nanocomposites also was significantly affected by processing speed. For example, mineralization curves for the PBSA/MLS combinations processed at 60 rpm were characterized by longer lag periods, slower mineralization kinetics (requiring longer times to achieve the 60% ThCO<sub>2</sub> threshold for biodegradable polymers), and lower respiratory quotients than the

nanocomposites processed at slower speeds. In addition, total net mineralization of the nanocomposites processed at 60 rpm was generally lower than for comparable nanocomposites processed at slower speeds, though this difference was significant for only the PBSA/MLS 1856. PBSA-based nanocomposites incorporating a mix of MLS 1855 and starch (1:1 w/w) produced films that were particularly affected by processing speed. Films processed at 20 rpm were not significantly affected by starch additions. Conversely, the incorporation of starch in the nanocomposites had a significant effect on the rate of mineralization of films processed at 60 rpm, though total net mineralization remained about the same. Mineralization of the PBSA/MLS nanocomposites in a standard soil environment produced no phytotoxic effects. Together with the mineralization data, these results demonstrate that the PBSA/MLS nanocomposites can be considered slowly biodegradable, environmentally friendly biobased materials that can be disposed of in the soil environment.

**Acknowledgments:** We thank the Army's Environmental Quality Basic Research Program for the funding of this research. We also acknowledge Dr. Bert Powell, Mr. Randy Chapman, and Antonio Gonzalez of Southern Clay Products for the nanoparticle and X-ray data. We also acknowledge Jeanne Lucciarini, Matthew Martez, Amanda Firtzgerald, Sarah Schirmer, and Elizabeth Welsh all who worked at the U.S. Army Natick Soldier Center and helped on the processing, thermal analysis, and mechanical testing of these samples. A special thank you is extended to Elizabeth Welsh for milling the PBSA into powder. Also, thank you to David Ziegler for the TEM images.

## References

1. D. Kaplan, J. M. Mayer, D. Ball, J. McCassie, A. L. Allen, and P. Stenhouse, *Biodegradable Polymer and Packaging*, edited by C. Ching, D. Kaplan, and E. Thomas (1993), pp. 1–51.
2. J. M. Mayer and D. L. Kaplan, *Trends Polym. Sci.* 2, 227 (1994).
3. R. Wool and X. S. Sun, (eds.), *Bio-Based Polymers and Composites*, Elsevier Academic Press, Burlington, MA (2005).
4. J. Fritz, U. Link, and R. Braun, *Starch-Starke* 53, 105 (2001).
5. White House Executive Order # 13134 (1999).
6. C. J. Weber (ed.), *Biobased Packaging Materials for the Food Industry*, The Royal Veterinary Agricultural University, Frederiksberg, Denmark (2000).
7. B. Miller, *Plastics Formulating Compounding* 3, 30 (1997).
8. A. Okada and A. Usuki, Hybrid organic-inorganic composites. *ACS Symp. Ser.* 585, 55 (1995).
9. E. P. Giannelis, *Adv. Mater.* 8, 29 (1996).
10. E. P. Giannelis, *Appl. Organomet. Chem.* 12, 675 (1998).
11. T. J. Pinnavaia and G. W. Beall (eds.), *Polymer Nanocomposites*, John Wiley & Sons Publishing, New York (2001).
12. G. H. Hu and L. F. Feng, *Macromol. Symp.* 195, 303 (2003).
13. J. Ratto, P. Stenhouse, M. Auerbach, J. Mitchell, and R. Farrell, *Polymer* 40, 6777 (1999).
14. T. Shioozono and J. Hino, Jpn. Kokai Tokyo Koho Patent, JP 09137069 A@070527 and 09294482 A2 97118 (1996).
15. T. Fujumaki, *Polym. Degradation Stability* 59, 209 (1998).

16. E. Takiyama and T. Fujumaki, *PACIFICHEM 95*, Honolulu, HI (1995).
17. J. G. Zeikus, M. K. Jain, and P. Elankovan, *Appl. Microbiol. Biotechnol.* 51, 545 (1999).
18. G. X. Chen and J. Yoon, *J. Polym. Sci., Part B: Polym. Phys.* 43, 817 (2005).
19. G. X. Chen, E. S. Kim, and J. S. Yoon, *J. Appl. Polym. Sci.* 98, 1727 (2005).
20. G. X. Chen and J. S. Yoon, *Polym. Int.* 54, 939 (2005).
21. S. S. Ray, M. Bousmina, and K. Okamoto, *Macromol. Mater. Eng.* 290, 759 (2005).
22. S. S. Ray and M. Bousmina, *Polymer* 46, 12430 (2005).
23. S. S. Ray, K. Okamoto, and M. Okamoto, *Macromolecules* 36, 2355 (2003).
24. K. Okamoto, S. S. Ray, and M. Okamoto, *J. Polym. Sci., Part B: Polym. Phys.* 41, 3160 (2003).
25. S. S. Ray, K. Okamoto, P. Maiti, and M. Okamoto, *J. Nanosci. Nanotechnol.* 2, 171 (2002).
26. Y. Someya, T. Nakazato, N. Teramoto, and M. Shibata, *J. Appl. Polym. Sci.* 91, 1463 (2004).
27. M. Shibata, *Kobunshi Kako* 52, 556 (2003).
28. S. R. Lee, H. M. Park, H. Lim, T. Kang, X. Li, W. J. Cho, and C. S. Ha, *Polymer* 43, 2495 (2002).
29. T. Mitsunaga, K. Okada, Y. Nagase, and T. Kimura, *Seikei Kako* 14, 604 (2002).
30. C. H. Lee, S. T. Lim, Y. H. Hyun, H. J. Choi, and M. S. Jhon, *J. Mater. Sci. Lett.* 22, 53 (2003).
31. S. T. Lim, C. H. Lee, H. J. Choi, and M. S. Jhon, *J. Polym. Sci., Part B: Polym. Phys.* 41, 2052 (2003).
32. S. T. Lim, C. H. Lee, H. Choi, and M. S. Jhon, Abstracts of Papers, 224th ACS National Meeting, Boston, MA, USA (2002).
33. S. Lim, C. H. Lee, H. J. Choi, and M. S. Jhon, *Polym. Prepr., Am. Chem. Soc., Div. Polym. Chem.* 43, 1286 (2002).
34. S. T. Lim, Y. H. Hyun, H. J. Choi, and M. S. Jhon, *Chem. Mater.* 14, 1839 (2002).
35. S. T. Lim, Y. H. Hyun, H. J. Choi, and M. S. Jhon, *Polymer Preprints* 42, 640 (2001).
36. R. Bartha and D. Pramer, *Soil Sci.* 100, 68 (1965).
37. American Society for Testing and Materials. Annual Book of ASTM Standards. ASTM, West Conshohocken, PA, Vol. 08-03, Standard D 5988 (2001).
38. CoHort, CoStat Statistical Software, Version 6.1. CoHort Software: Minneapolis, MN (2001).
39. R. E. Farrell, T. C. Adameczyk, D. C. Broe, J. S. Lee, B. L. Briggs, R. A. Gross, S. P. McCarthy, and S. Goodwin, *Biopolymers from Polysaccharides and Agroproteins*, edited by R. A. Gross and C. Scholz, ACS Symposium Series 786, American Chemical Society, Washington, DC, pp. 337-375 (2000).
40. U.S. Environmental Protection Agency. 1998a. Fate, Transport and Transformation Test Guidelines OPPTS 835.3110 Ready Biodegradability. U.S. EPA 712-C-98-076, Washington, DC (1998).
41. U.S. Environmental Protection Agency. 1998b. Fate, Transport and Transformation Test Guidelines OPPTS 835.3300 Soil Biodegradation. U.S. EPA 712-C-98-088, Washington, DC (1998).
42. F. Zucconi, M. Forte, A. Monaco, and M. Bertoldi, *Biocycle* (1981).
43. P. B. Legee and W. H. Thompson (eds.), *Test Methods for the Examination of Composting and Compost*, The U.S. Composting Council, Bethesda, MD, Vol. 22, p. 27 (1997).
44. J. W. Tukey, *Exploratory Data Analysis*, Addison-Wesley, Reading, MA (1977).
45. J. H. Zar, *Biostatistical Analysis*, 2nd edn., McGraw-Hill, New York (1984).
46. C. Thellen, C. Orroth, D. Froio, D. Ziegler, R. Farrel, N. D'souza, J. Lucciarini, and J. Ratto, *Polymer* 46, 11 716 (2005).
47. E. Culhane, D. Froio, C. Thellen, C. Orroth, J. Lucciarini, and J. Ratto, *J. Soc. Plastics Eng. Annu. Technical Conf. Proc.* 63, 1916 (2005).
48. N. E. Sharabi and R. Bartha, *Appl. Environ. Microbiol.* 59, 1201 (1993).

Received: 26 July 2006. Revised/Accepted: 12 September 2006.

AMERICAN  
SCIENTIFIC  
PUBLISHERS